Optimal Coastal Adaptation Strategies Under Deep Uncertainty: Risk Management via Confidence-Based Exploration

Johan Jönsson & Christian

December 29, 2025

1 Introduction

The design of coastal infrastructure in the Anthropocene requires a rigorous treatment of deep uncertainty, characterized by the interplay between two forms of uncertainty: the *epistemic* uncertainty regarding the future trajectory of the climate system and the *aleatoric* uncertainty inherent in stochastic extreme sea-level (ESL) events. While climate change is expected to exacerbate extreme sea levels, quantifying these shifts remains computationally challenging due to the structural ambiguity of climate drivers. Consequently, coastal hazard profiles are often defined not by mean states, but by the thickening tails of flood distributions—processes that are non-stationary and highly sensitive to epistemic errors in projections.

From an economic perspective, reliance on expected values or median projections can lead to a systematic underestimation of potential damages. Abadie et al. [2019] argue that risk tolerance should be defined by the upper tails of the damage distribution rather than central estimates, utilising measures such as Expected Shortfall (ES) to capture losses in low-probability, high-impact scenarios. Neglecting these tail events is tantamount to underestimating risk, as damages in the upper tail can be significantly higher than mean values [Abadie et al., 2019]. To operationalize these concepts, we utilize the standardized damage and protection cost curves provided by Prahl et al. [2018], which allow for comparative assessments of adaptation costs despite the inherent uncertainties in local asset values.

However, optimizing protection levels under such compounded uncertainty is analytically intractable using standard minimization techniques, as it requires integrating over a wide variety of heavy-tailed distributions. To address this optimization challenge, we adopt a machine learning framework based on the Multi-Armed Bandit (MAB) problem. Unlike traditional methods that attempt to pre-calculate the full damage landscape, the MAB framework allows for sequential decision-making that balances exploration (gathering data on uncertain hazard tails) and exploitation (identifying the optimal design).

However, we primarily used *Pure Exploration* algorithms. As detailed by Lattimore and Szepesvári [2020], pure exploration—specifically the fixed-confidence best-arm identification setting—is distinct from standard regret minimization; the goal is not to maximize cumulative reward during the learning phase, but to identify the optimal design (arm) with high probability using the fewest number of samples. This is particularly well-suited for infrastructure planning where the "cost" of exploration is computational rather than physical. We contrast this primary method with a side comparison using *Dueling Bandits*, a variation discussed in the broader bandit literature [Lattimore and Szepesvári, 2020], which relies on pairwise comparisons rather than absolute reward estimates to identify the optimal design.

2 Data sources and threshold selection

2.1 Climate ensemble

To represent uncertainty in future mean sea-level (MSL) rise, we use the IPCC AR6 sea-level projections data set, distributed via Zenodo and documented in the Rutgers "Guide to the IPCC AR6 Sea Level Projections" repository Garner et al. [2021]. This data set contains the sea-level projections associated with the IPCC Sixth Assessment Report and includes the full set of Monte Carlo samples for global mean sea-level projections, as well as summary relative sea-level projections, both with and without the AR6 estimate of background sea-level process rates.

For our site-specific hazard model, we extract the regional relative sea-level projections at the tide-gauge location closest to Halmstad (Varberg) and interpolate them to annual time steps. Each ensemble member $X_t^{(m)}$ then provides an annual MSL trajectory over the planning horizon ($t = 1, \ldots, n$), implicitly combining contributions from ocean thermal expansion, land ice, and other processes represented in the AR6 framework. The spread of these trajectories captures structural and scenario uncertainty in future sea-level change, and in our Bayesian model the AR6 ensemble serves as an empirical prior $p_{\mathrm{AR6}}(X)$ for the latent climate covariate.

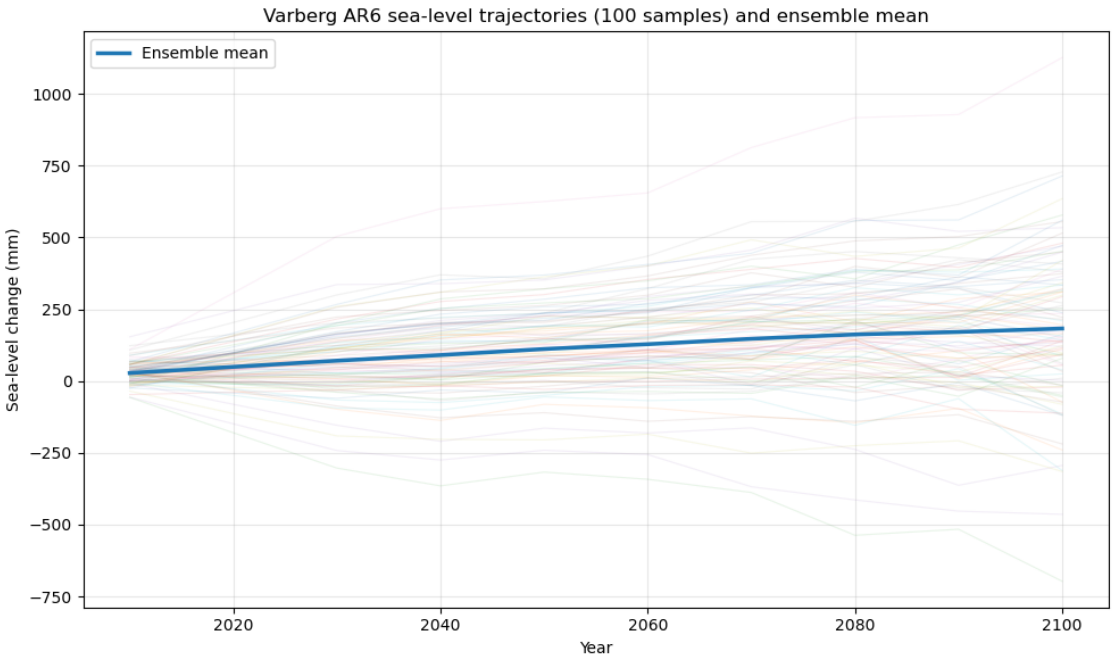

Figure 1: AR6 sea-level ensemble for Varberg. Thin coloured lines show a random subset of 100 simulated MSL trajectories from the IPCC AR6 data set, and the thick blue line denotes the ensemble mean.

2.2 SMHI sea-level observations

Observational constraints are derived from the Swedish Meteorological and Hydrological Institute (SMHI) tide gauge at Halmstad. Hourly sea-level observations are available in the SMHI open oceanographic database at station *Halmstad Sjöv* (station number 35115). The time series provides hourly sea-level measurements from 2009 onwards; the hourly sea-level observations at Halmstad's tide gauge (station 35115) are publicly available via SMHI's database. Figure2 illus-

trates the raw hourly time series from 2010–2024. Seasonal cycles and occasional extreme events are evident. To model flood extremes, we decluster this series: events are identified when the level exceeds a high threshold u and are separated by gaps longer than 24 hours, yielding independent peaks-over-threshold exceedances $Y_{t,i}$ for each storm year t.

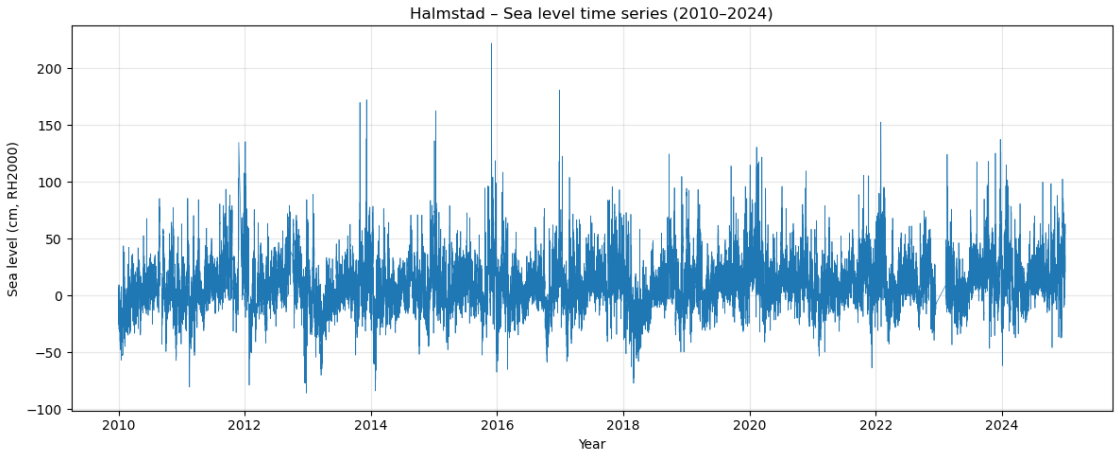

Figure 2: Hourly sea-level time series at Halmstad (2010–2024).

2.3 Threshold selection

Selecting an appropriate threshold u is critical: it must be high enough that exceedances follow a Generalised Pareto distribution (GPD) but low enough to retain sufficient data. We assess candidate thresholds using the mean residual life (MRL) plot and estimates of the GPD shape parameter $\xi(u)$. For a stationary GPD model, the MRL plot $\mathrm{E}[X \mid X > u]$ versus u should be approximately linear. As shown in Figure 3, the empirical mean excess function is roughly linear above 60 cm and remains stable up to about 80 cm. Similarly, Figure 4 displays point estimates of the GPD shape parameter against threshold together with 95 % uncertainty bands. The estimates fluctuate around zero for thresholds between 60 and 90 cm. Based on these diagnostics, we adopt $u = 60$ cm as the threshold.

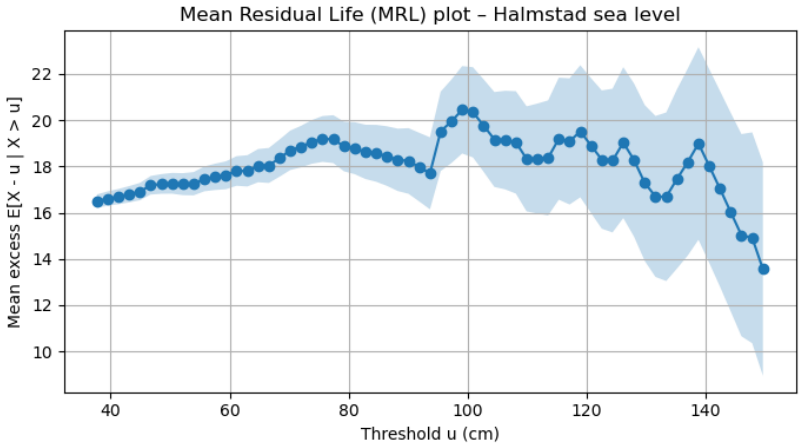

Figure 3: Mean residual life (MRL) plot for the Halmstad sea-level data. The mean excess $\mathrm{E}[X - u \,|\, X > u]$ is plotted against the threshold u with pointwise 95 % confidence intervals. Approximate linearity above 60 cm suggests suitability of a GPD model for exceedances.

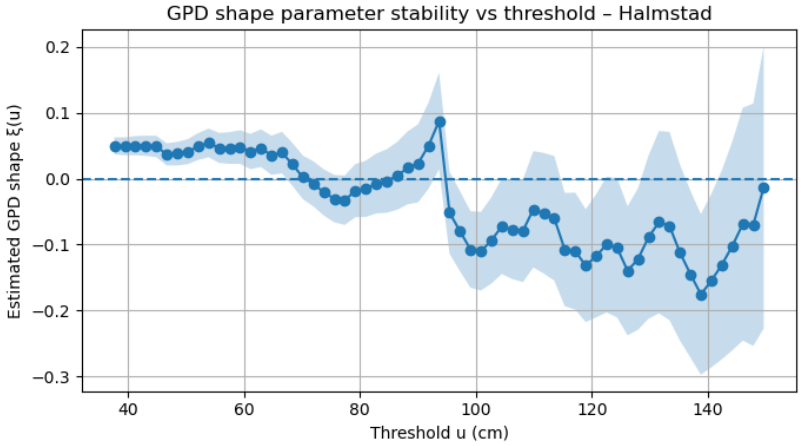

Figure 4: Stability of the GPD shape parameter estimate versus threshold. The solid line shows the maximum-likelihood estimate of $\xi(u)$, and the shaded band corresponds to 95 zero for thresholds between 60 and 90 cm support the choice of $u = 60$ cm.

2.4 Bayesian simulator, uncertainty and validation

After declustering and thresholding, the exceedances $(N_t, Z_{t,i})$ are modelled as a Poisson–GPD point process conditional on the latent climate covariate $X_t^{(m)}$. Formally, for a given MSL path $X^{(m)}$ and parameter vector $\theta = (\eta_0, \eta_1, \sigma, \xi)$ we assume

$$N_t \mid X_t^{(m)}, \theta \sim \text{Poisson}\big(\Lambda_t^{(m)}\big), \qquad \log \Lambda_t^{(m)} = \eta_0 + \eta_1 X_t^{(m)},$$

and, conditionally on N_t,

$$Z_{t,i} \mid \theta \sim \text{GPD}(\sigma, \xi), \qquad i = 1, \ldots, N_t.$$

Bayesian treatment of aleatoric and epistemic uncertainty. Let $\mathcal{D} = \{N_t, Z_{t,i} : t = 1, \ldots, T,\ i = 1, \ldots, N_t\}$ denote the observed exceedance counts and excesses above the threshold u. The model is cast in a Bayesian framework by treating both the parameters and the climate projections as random:

$$p(\mathcal{D} \mid \theta, X)\, p(\theta)\, p_{\mathrm{AR6}}(X).$$

Here

- *Aleatoric uncertainty* (intrinsic randomness) comes from the Poisson counts N_t and the GPD excesses $Z_{t,i}$ for a given (θ, X). This is encoded directly in the likelihood $p(\mathcal{D} \mid \theta, X)$.
- *Epistemic uncertainty* (lack of knowledge) enters through the posterior over θ and through the unknown future MSL path X. We estimate $p(\theta \mid \mathcal{D})$ via MCMC and use the AR6 ensemble $p_{\mathrm{AR6}}(X)$ as an empirical prior over climate trajectories.

The simulator then samples from the posterior predictive distribution of future exceedance processes $\tilde{\mathcal{D}}$,

$$p(\tilde{\mathcal{D}} \mid \mathcal{D}) = \iint p(\tilde{\mathcal{D}} \mid \theta, X)\, p(\theta \mid \mathcal{D})\, p_{\mathrm{AR6}}(X)\, d\theta\, dX,$$

so that both aleatoric and epistemic components are propagated into future extreme sea-level behaviour.

Implementation in PyMC and AR6 mixture likelihood. We implement posterior inference for $\theta = (\eta_0, \eta_1, \sigma, \xi)$ in the probabilistic programming library PyMC Abril-Pla et al. [2023]. Since the latent MSL path X_t is not observed directly, but only through the AR6 ensemble $\{X^{(m)}\}_{m=1}^{M}$, the marginal likelihood for the exceedance data $\mathcal{D} = \{N_t, Z_{t,i}\}$ integrates over X:

$$p(\mathcal{D} \mid \eta_0, \eta_1, \sigma, \xi) = \int p(\mathcal{D} \mid X, \eta_0, \eta_1, \sigma, \xi)\, p_{\mathrm{AR6}}(X)\, dX.$$

Approximating p_{AR6} by the empirical distribution of the M AR6 paths gives the finite mixture

$$p(\mathcal{D} \mid \eta_0, \eta_1, \sigma, \xi) \approx \frac{1}{M} \sum_{m=1}^{M} \prod_{t} \mathrm{Poisson}\big(N_t \mid \Lambda_t^{(m)}\big) \cdot \prod_{t,i} f_{\mathrm{GPD}}(Z_{t,i} \mid \sigma, \xi),$$

where $\Lambda_t^{(m)} = \exp(\eta_0 + \eta_1 X_t^{(m)})$ and f_{GPD} is the GPD density for the excesses. Because the GPD part does not depend on m, this simplifies to

$$p(\mathcal{D} \mid \eta_0, \eta_1, \sigma, \xi) \approx \left[\prod_{t,i} f_{\mathrm{GPD}}(Z_{t,i} \mid \sigma, \xi)\right] \cdot \prod_{t} \left[\frac{1}{M} \sum_{m=1}^{M} \mathrm{Poisson}\big(N_t \mid \Lambda_t^{(m)}\big)\right].$$

In practice we work with the log-likelihood (up to an additive constant), implemented in PyMC using a numerically stable log-sum-exp over AR6 paths:

$$\ell(\eta_0, \eta_1, \sigma, \xi) \approx \sum_{t,i} \log f_{\mathrm{GPD}}(Z_{t,i} \mid \sigma, \xi) + \sum_{t} \log \left[\frac{1}{M} \sum_{m=1}^{M} \exp\big(\log \mathrm{Poisson}\big(N_t \mid \Lambda_t^{(m)}\big)\big)\right].$$

This custom log-likelihood is supplied to the NUTS sampler in PyMC, which draws posterior samples from $p(\theta \mid \mathcal{D})$ under the AR6 mixture representation.

Step 1: Draw a climate trajectory and parameters. For each simulation replicate $s = 1, \ldots, S$ we:

1. Sample one AR6 MSL path $X_t^{(m_s)}$, $t = 2025, \ldots, 2100$, from the regional AR6 ensemble (Varberg/Halmstad). This is one plausible realization of future climate forcing, capturing structural and scenario uncertainty (epistemic).

2. Sample model parameters
$$\theta^{(s)} = (\eta_0^{(s)}, \eta_1^{(s)}, \sigma^{(s)}, \xi^{(s)})$$
from the joint posterior $p(\theta \mid \text{Data})$. This step carries parameter uncertainty (epistemic) into the simulator.

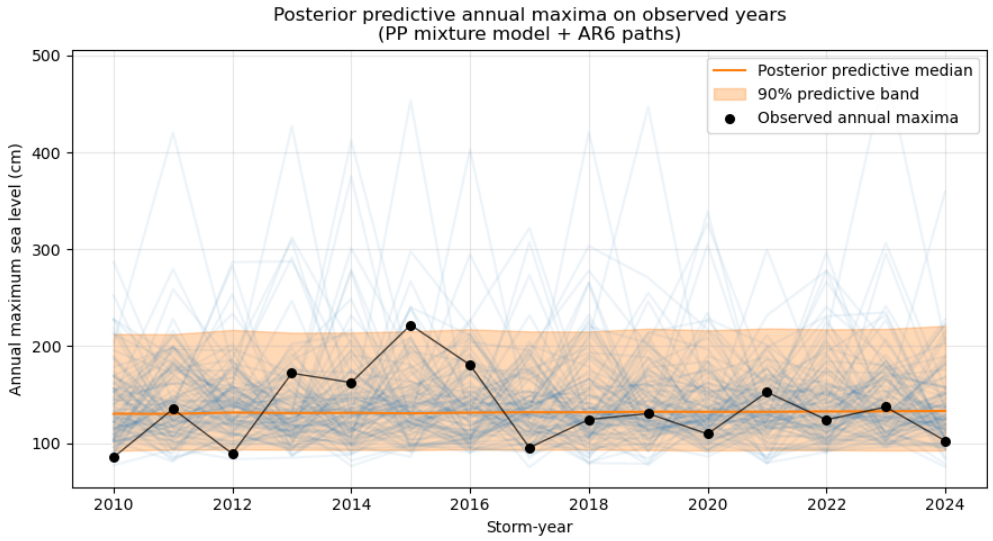

Figure 5: Posterior predictive check for annual maximum sea levels at Halmstad (2009–2024). Black dots denote observed maxima; the orange line and blue band show the median and 90% predictive interval from the fitted simulator.

Step 2: Simulate exceedances in each year. Conditional on the sampled climate path $X^{(m_s)}$ and parameters $\theta^{(s)} = (\eta_0^{(s)}, \eta_1^{(s)}, \sigma^{(s)}, \xi^{(s)})$, we evolve the point process over years $t = 1, \ldots, n$ of the planning horizon:

1. *Poisson rate.* For each year t compute the expected number of threshold exceedances
$$\Lambda_{s,t} = \exp\big(\eta_0^{(s)} + \eta_1^{(s)} X_t^{(m_s)}\big).$$

2. *Event count (aleatoric).* Draw the number of peaks above the threshold $u = 60\,\text{cm}$ in year t,
$$N_{s,t} \sim \text{Poisson}\big(\Lambda_{s,t}\big).$$

3. *Magnitudes (aleatoric).* Given $N_{s,t}$, draw excesses $Z_{s,t,i}$ above u from $\text{GPD}(\sigma^{(s)}, \xi^{(s)})$. Using inverse transform sampling, for $U \sim \text{Unif}(0,1)$,
$$Z = \begin{cases} -\sigma^{(s)} \log(1-U), & \text{if } |\xi^{(s)}| < 10^{-6}, \\ \dfrac{\sigma^{(s)}}{\xi^{(s)}}\big((1-U)^{-\xi^{(s)}} - 1\big), & \text{otherwise.} \end{cases}$$

and we set $Z_{s,t,i} = Z$ for $i = 1, \ldots, N_{s,t}$.

Step 3: Annual maxima and posterior predictive band. For each episode s and year t we form the simulated annual maximum flood level (relative to RH2000) as

$$F_{s,t} = \begin{cases} u + \max_{1 \le i \le N_{s,t}} Z_{s,t,i}, & N_{s,t} > 0, \\ \text{annual maximum at or below } u, & N_{s,t} = 0, \end{cases}$$

where in practice the second case uses the observed sub-threshold maximum from the hourly record. Across the ensemble $\{F_{s,t}\}_{s=1}^{S}$ we then compute, for each year t,

- the posterior predictive median $\tilde{F}_t$, and
- a central 90% predictive band (5th and 95th percentiles).

Figure 6 compares these summaries with the observed annual maxima at Halmstad (2009–2024). The black dots (data) lie comfortably inside the 90% predictive band, indicating that the Poisson–GPD model with AR6 latent forcing reproduces both the level and interannual variability of extremes.

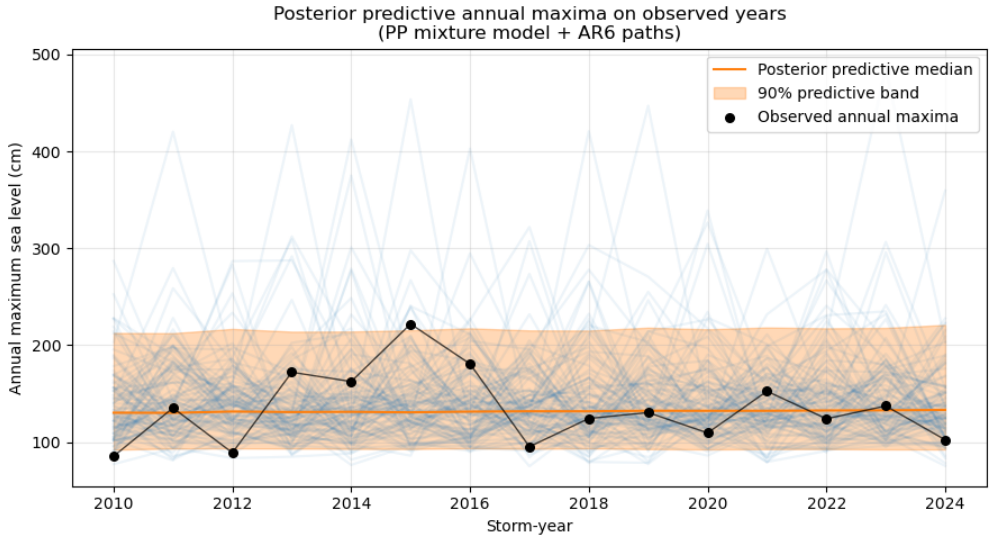

Figure 6: Posterior predictive check for annual maximum sea levels at Halmstad (2009–2024). Black dots denote observed maxima; the orange line and blue band show the median and 90% predictive interval from the fitted simulator.

Repeating this for $S = 100{,}000$ Monte Carlo scenarios yields an empirical posterior predictive distribution of total costs at a given defence height. Figure 7 shows this distribution, at the optimal height using dueling bandits, $h^\star = 2.50\,\text{m}$: the bulk of realizations forms a narrow mode around the posterior mean (dashed line), while a small subset of scenarios generates a heavy right tail of rare but very expensive flood sequences. The zoom into the upper 1% in Figure 8 highlights these tail events and the 99th percentile cost threshold used in our risk metrics.

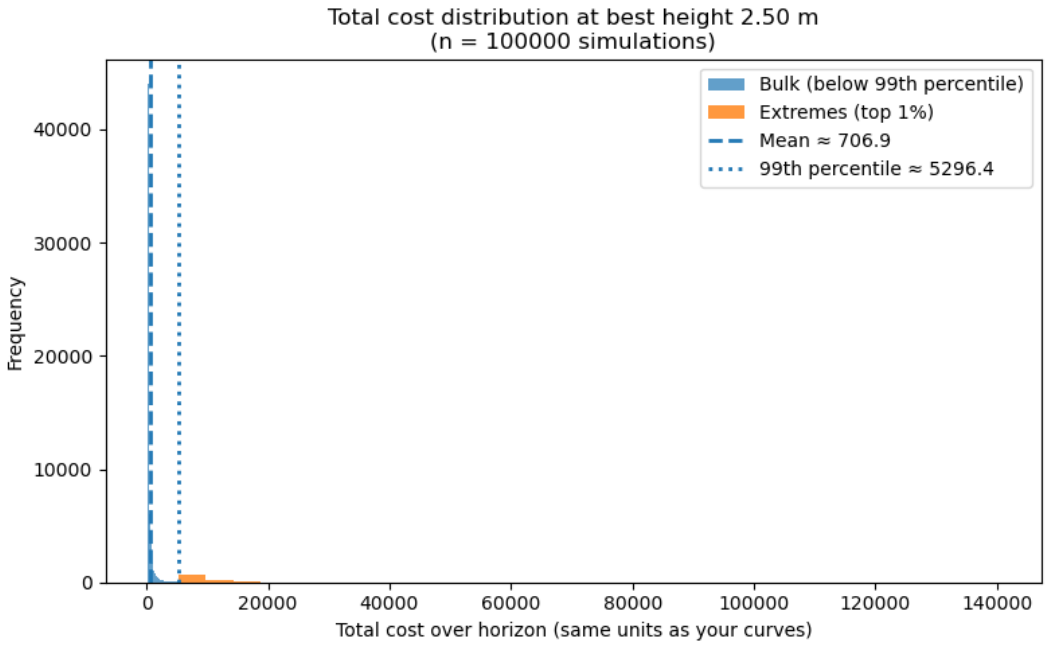

Figure 7: Simulated distribution of total discounted costs at the selected defence height $h^\star = 2.50\,\mathrm{m}$ over the 2025–2100 horizon ($S = 100{,}000$ scenarios). The dashed line marks the posterior mean cost, and the dotted line the 99th percentile, separating the bulk from the most extreme realizations.

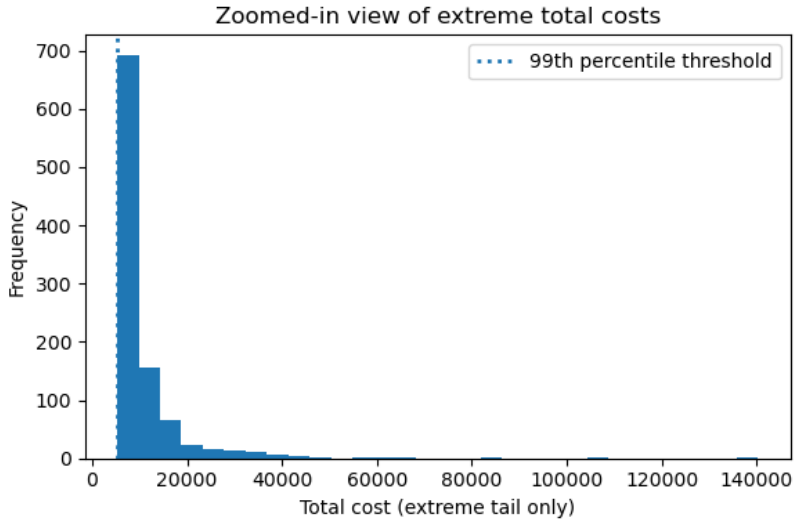

Figure 8: Zoomed-in view of the upper tail of the total cost distribution (top 1% of scenarios). The vertical dotted line shows the estimated 99th percentile of total costs, a high-impact, low-probability loss benchmark.

Overall, this Bayesian simulator combines aleatoric uncertainty from the stochastic flood-generating process with epistemic uncertainty in both model parameters and future climate forcing. By sampling from the joint posterior over (θ, X) and propagating through to annual maxima and costs, we obtain internally consistent posterior predictive bands for future extremes and a full

distribution of aggregated costs under any proposed coastal defence strategy.

2.5 Parameter Calibration

Figure 9 presents the calibration results for the model parameters $\theta = (\eta_0, \eta_1, \sigma, \xi)$. The comparison between the broad prior distributions and the narrower posterior histograms demonstrates how the observational data from Halmstad has constrained the parameter space.

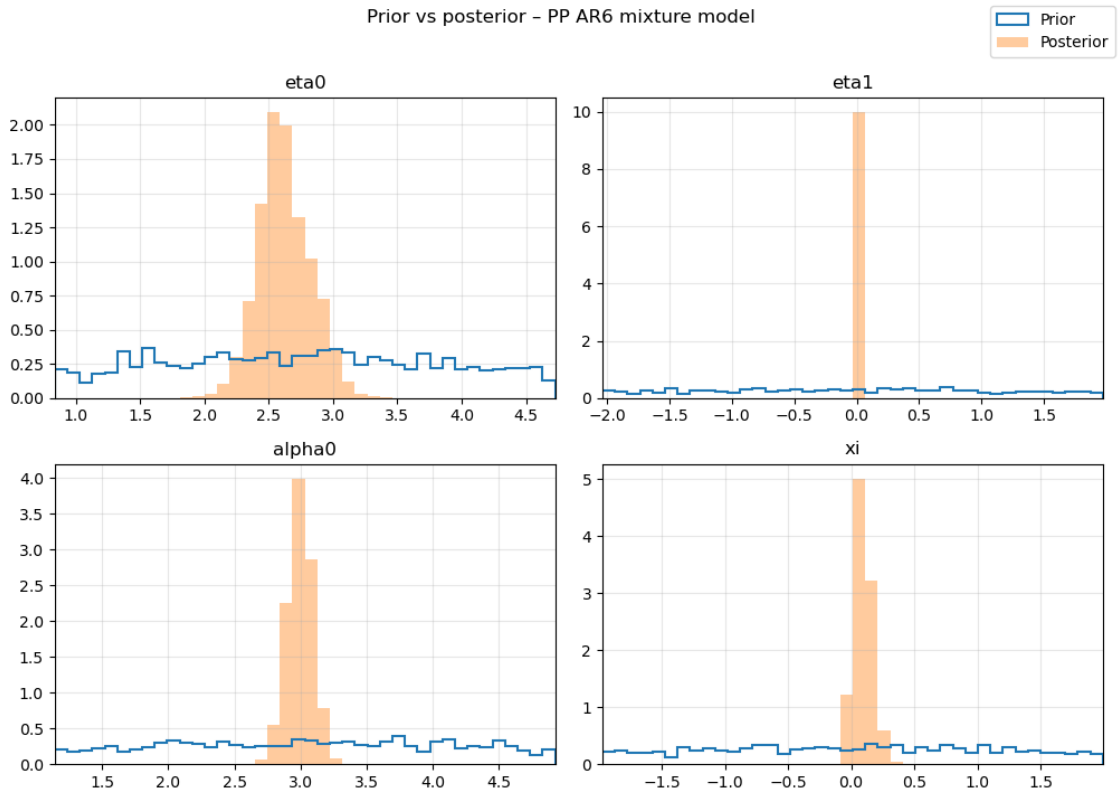

Figure 9: Prior (blue outline) versus posterior (orange fill) distributions for the model parameters. The plots show the Poisson process coefficients (η_0, η_1) and the GPD parameters (σ denoted as alpha0, and ξ).

3 Risk-neutral objective and confidence-based pure exploration

3.1 Theoretical explanation

We begin by formalising the risk-neutral design objective and then show how it fits naturally into the mathematical framework of *pure-exploration bandits*. Consider a finite, ordered set of admissible levee heights $\mathcal{H} = \{h_0 < h_1 < \cdots < h_K\}$. For a given design height $h \in \mathcal{H}$ and a planning horizon of n years, we write $C_n(h)$ for the present value of all capital and maintenance costs over the n-year horizon; we treat $C_n(h)$ as a deterministic, known function of h, obtained from cost curves. Uncertainty enters through the annual maximum flood heights. Let $F = (F_1, \ldots, F_n)$ denote the vector of annual maxima over the n-year horizon, viewed as a random element generated by the hazard model together with the priors on (θ, X). A *damage function* $D(F \mid h)$ maps a flood trajectory F and a design height h to the total discounted damage cost over the n-year horizon;

we assume $D(F \mid h) \geq 0$ and that it is non-decreasing in each flood height component. It is often convenient to imagine $D(F \mid h)$ as a sum of one-year damages: for each year $t = 1, \ldots, n$, there is a one-year damage $d_t(F_t \mid h) \geq 0$ such that

$$D(F \mid h) \;=\; \sum_{t=1}^{n} d_t(F_t \mid h).$$

We assume that there is a physically meaningful bound $d_{\max} < \infty$ on the *one-year* damage, uniform over years, heights and flood realisations, i.e.

$$0 \;\leq\; d_t(F_t \mid h) \;\leq\; d_{\max} \qquad \text{for all } t = 1, \ldots, n,\; F,\; h \in \mathcal{H}.$$

Summing over t then yields a deterministic, distribution-free bound on the total n-year damage:

$$0 \;\leq\; D(F \mid h) \;\leq\; n\, d_{\max} \;=:\; D_{\max} \qquad \text{for all } F,\; h \in \mathcal{H}.$$

Given the joint distribution of F induced by the hazard model and priors, the *risk-neutral expected total cost* of choosing height h is

$$\mu_h \;:=\; C_n(h) + \mathbb{E}\big[D(F \mid h)\big], \tag{1}$$

and the risk-neutral decision problem is to pick an h that minimises μ_h:

$$h^* \;:=\; \arg\min_{h \in \mathcal{H}} \mu_h.$$

In our setting, the distribution of F is defined by a mixture over climate pathways and extreme-value parameters, so the exact values of the expectations μ_h cannot be computed analytically. Instead, we approximate them via Monte-Carlo simulation. A single Monte Carlo *episode* consists of simulating one n-year flood trajectory $F_s = (F_{s,1}, \ldots, F_{s,n})$ from the hazard model and then evaluating the resulting total damage at every candidate height using the same realised flood path. Formally, in episode $s \geq 1$ we draw F_s and compute

$$Y_{s,h} \;:=\; D(F_s \mid h), \qquad h \in \mathcal{H},$$

so that each $Y_{s,h}$ is a random draw from the damage distribution associated with height h, and by the one-year bound above we have $0 \leq Y_{s,h} \leq D_{\max}$ almost surely for every s and h. The common use of F_s across all heights h corresponds to the standard variance-reduction device of *common random numbers*. After S independent episodes we obtain S i.i.d. samples $\{Y_{s,h}\}_{s=1}^{S}$ for each fixed height h, and we estimate μ_h by the sample average

$$\hat{\mu}_h(S) \;:=\; C_n(h) \;+\; \frac{1}{S} \sum_{s=1}^{S} Y_{s,h}, \qquad S \geq 1. \tag{2}$$

Because $C_n(h)$ is deterministic, the estimation error is entirely due to the random damage term:

$$\hat{\mu}_h(S) - \mu_h \;=\; \frac{1}{S} \sum_{s=1}^{S} \big(Y_{s,h} - \mathbb{E}[Y_{1,h}]\big), \qquad \mathbb{E}[Y_{1,h}] = \mathbb{E}[D(F \mid h)].$$

This simulation scheme fits naturally into the theory of *pure-exploration multi-armed bandits*. In that framework (see, for example, Lattimore and Szepesvári [2020]), one is given a finite set

of *arms* with unknown mean losses or rewards μ_h, and the learner interacts with the system in rounds. In round s, the learner chooses an arm (or, as in our case, implicitly observes all arms at once), receives a noisy sample whose distribution depends on the chosen arm, and then uses the accumulated data to decide whether to continue experimenting or to stop and recommend an arm. A *pure-exploration* problem is one in which the running losses or rewards generated during the experiment do not enter the objective; only the final recommendation matters. A standard formalisation is the *fixed-confidence* setting: the user specifies a confidence level $\delta \in (0,1)$, and the algorithm chooses (i) a sampling policy π describing how observations are collected over time, (ii) a random stopping time τ (measured in Monte Carlo episodes) at which experimentation is halted, and (iii) a recommendation rule ψ that returns one arm based on the data up to time τ. The algorithm is called δ-*correct* (or δ-sound) if

$$\mathbb{P}\big(\tau < \infty,\ \psi \neq h^*\big) \ \leq\ \delta,$$

that is, with probability at least $1-\delta$ the recommended arm is truly optimal whenever the algorithm stops. A crucial feature of pure exploration is that the stopping time τ is a genuine random variable that depends on the realised data: in "easy" instances with large gaps between arms, the algorithm will tend to stop quickly, whereas in "hard" instances with nearly tied arms, more episodes are needed, but in all cases the correctness guarantee remains the same.

In our levee design problem, each height $h \in \mathcal{H}$ plays the role of an arm, its unknown mean loss is the expected risk-neutral cost μ_h in (1), and a single Monte Carlo episode consists of simulating a flood trajectory F_s and observing the bounded loss vector $(Y_{s,h})_{h\in\mathcal{H}}$, with $0 \leq Y_{s,h} \leq D_{\max}$ almost surely. Because every episode gives us one new observation for *every* arm, the sampling policy π is especially simple: we do not need to decide which arm to play at each step, we simply keep drawing new flood trajectories and updating the empirical means for all heights. The remaining questions are: how do we quantify the statistical uncertainty in the estimates $\hat{\mu}_h(S)$, and how do we use this uncertainty to construct a stopping time τ and recommendation rule ψ that are δ-correct?

The starting point is a concentration inequality for the Monte Carlo estimators. Fix a height $h \in \mathcal{H}$. The random variables $Y_{1,h}, Y_{2,h}, \dots$ are i.i.d. with mean $\mathbb{E}[Y_{1,h}]$ and are bounded in the interval $[0, D_{\max}]$. Classical results for bounded independent random variables, such as Hoeffding's inequality, then give for any $\varepsilon > 0$ and any $S \geq 1$,

$$\mathbb{P}\Big(\big|\hat{\mu}_h(S) - \mu_h\big| > \varepsilon\Big) \ =\ \mathbb{P}\Big(\Big|\frac{1}{S}\sum_{s=1}^{S} Y_{s,h} - \mathbb{E}[Y_{1,h}]\Big| > \varepsilon\Big) \ \leq\ 2\exp\Big(-\frac{2S\varepsilon^2}{D_{\max}^2}\Big), \tag{3}$$

because changing a single $Y_{s,h}$ can change the average by at most $D_{\max}/S$. Inequality (3) shows that, for each fixed height h and sample size S, the Monte Carlo error decays at the familiar $1/\sqrt{S}$ rate, with a universal constant $D_{\max}$ coming from the n-year damage bound. However, pure exploration requires a stronger, *uniform* control: we want one high-probability event on which *all* empirical means are close to their true means *for all sample sizes* simultaneously, because our stopping time τ is itself a random function of the data.

To obtain such a uniform control, we apply a union bound over heights and sample sizes. For any non-increasing sequence of tolerances $\{\varepsilon_S\}_{S\geq 1}$,

$$\mathbb{P}\Big(\exists S \geq 1,\ \exists h \in \mathcal{H} : \big|\hat{\mu}_h(S) - \mu_h\big| > \varepsilon_S\Big) \ \leq\ \sum_{S=1}^{\infty}\sum_{h\in\mathcal{H}} 2\exp\Big(-\frac{2S\varepsilon_S^2}{D_{\max}^2}\Big).$$

We now choose ε_S so that the right-hand side is at most the desired error probability δ. A convenient

explicit choice is to define, for each $S \geq 1$, the *confidence radius*

$$r(S) \;:=\; D_{\max}\sqrt{\frac{1}{2S}\log\Big(\frac{2|\mathcal{H}|\,S(S+1)}{\delta}\Big)}, \tag{4}$$

which makes the double sum

$$\sum_{S=1}^{\infty}\sum_{h\in\mathcal{H}} 2\exp\Big(-\frac{2Sr(S)^2}{D_{\max}^2}\Big)$$

bounded by δ. By the union bound, this implies that the *good event*

$$G \;:=\; \Big\{\forall S\geq 1,\ \forall h\in\mathcal{H}:\ \big|\hat{\mu}_h(S)-\mu_h\big|\leq r(S)\Big\}$$

has probability at least $1-\delta$. On G, every empirical mean $\hat{\mu}_h(S)$ lies inside a confidence interval of radius $r(S)$ around the true mean μ_h, and this holds *uniformly* over all heights and all sample sizes.

We are now ready to define a stopping rule and recommendation in the spirit of fixed-confidence pure-exploration bandit algorithms. After each episode $S \geq 1$, we compute the current empirical best height

$$\hat{h}(S) \;:=\; \arg\min_{h\in\mathcal{H}} \hat{\mu}_h(S),$$

breaking ties arbitrarily. We then ask whether the data collected so far are sufficient to declare $\hat{h}(S)$ optimal. Intuitively, we should stop when the "optimistic" estimate of the best arm is still better than the "pessimistic" estimates of all others. Using the confidence radii $r(S)$, this leads to the stopping time

$$\tau \;:=\; \inf\Big\{S\geq 1:\ \hat{\mu}_{\hat{h}(S)}(S)+r(S) \;<\; \hat{\mu}_h(S)-r(S) \text{ for all } h\in\mathcal{H}\setminus\{\hat{h}(S)\}\Big\}, \tag{5}$$

and when $\tau<\infty$ we set $\psi := \hat{h}(\tau)$ as the recommended height. The rule (5) is *purely exploratory*: we never use the current best arm to guide the physical system or to "exploit" low costs; we only keep simulating flood trajectories, updating the empirical means, and checking whether our confidence intervals separate the best arm from all competitors. The total number of episodes τ is random and automatically adapts to the difficulty of the instance.

To see why this procedure is δ-correct, restrict attention to the good event G, which has probability at least $1-\delta$. On G, the inequalities in (5) imply that for every competitor $h\neq\hat{h}(\tau)$ we have

$$\mu_{\hat{h}(\tau)} \;\leq\; \hat{\mu}_{\hat{h}(\tau)}(\tau)+r(\tau) \;<\; \hat{\mu}_h(\tau)-r(\tau) \;\leq\; \mu_h,$$

so $\mu_{\hat{h}(\tau)}<\mu_h$ for all $h\neq\hat{h}(\tau)$ and therefore $\hat{h}(\tau)=h^*$ whenever $\tau<\infty$. Hence, on G the algorithm never stops with a suboptimal recommendation, and we conclude that

$$\mathbb{P}\big(\tau<\infty,\ \psi\neq h^*\big) \;\leq\; \mathbb{P}(G^c) \;\leq\; \delta,$$

showing that our Monte Carlo procedure is a fixed-confidence, pure-exploration best-arm identification algorithm for the levee design problem. Finally, if we denote the *gaps* by $\Delta_h := \mu_h-\mu_{h^*}>0$ for $h\neq h^*$ and write $\Delta_{\min} := \min_{h\neq h^*}\Delta_h$, then a simple sufficient condition for (5) to hold is $r(S)\leq\Delta_{\min}/2$, which, via (4), is satisfied once S is on the order of

$$S \;\asymp\; \frac{D_{\max}^2}{\Delta_{\min}^2}\log\Big(\frac{|\mathcal{H}|}{\delta}\Big),$$

up to logarithmic factors in S. Thus, under the sole structural assumption of a bounded one-year damage (and hence a bounded n-year damage $D_{\max}$), we obtain a transparent, distribution-free sample-complexity guarantee for the *random* number of Monte Carlo episodes needed to identify the risk-neutral optimal levee height with confidence at least $1 - \delta$, in close analogy with the classical pure-exploration theory for best-arm identification in multi-armed bandits; see Chapter 33 of Lattimore and Szepesvári [2020] for a general introduction.

3.2 GPU based algorithmic implementation

Why we do not use CLT/normality. The Monte Carlo estimator (2) must be evaluated to high precision for each candidate height $h \in \mathcal{H}$. Even though one-year damages are bounded (so the variance of $Y_{s,h}$ is finite), the induced n-year damage can be heavy-tailed. In such cases the classical central limit theorem is technically valid but converges very slowly.

In practice this means that to (i) justify a Gaussian approximation for the sample mean, (ii) check its adequacy via normality tests, and (iii) obtain tight confidence intervals from that approximation, we would need extremely large sample sizes and would have to store a substantial fraction of the sample history (or at least enough moments and order statistics) for each height. For the large sample sizes we need in this problem this CLT-based workflow becomes prohibitive: it is too slow (serial CPU) and too memory-hungry (storing $O(S \times |\mathcal{H}|)$ data). Instead we exploit the simple boundedness assumption and use Hoeffding-style concentration inequalities, which only require running sums and counts. This leads directly to a streaming, distribution-free algorithm that is a better match for our heavy-tail regime.

High-level GPU algorithm The GPU implementation is organised as a streaming algorithm over Monte Carlo batches [joensson12, 2025]. At a high level:

- **Inputs:**
  - candidate heights $\mathcal{H}_{\text{eff}} = \{h_1, \ldots, h_C\}$,
  - planning horizon n_{years},
  - posterior draws $(\eta_0^{(b)}, \eta_1^{(b)}, \sigma^{(b)}, \xi^{(b)})$ and AR6 paths $X^{(b)}$,
  - batch size `batch_size` and check interval `check_every`,
  - damage curves (Prahl et al.) and cost curves $C_n(h)$.
- **State (on host):**
  - running totals `cum_damage`$[h]$ for each $h \in \mathcal{H}_{\text{eff}}$,
  - episode counter S (number of simulated scenarios so far).
- **Loop over batches:** while not stopped, send a batch of posterior draws and AR6 paths to the GPU, simulate, update `cum_damage`, discard the batch, and occasionally check the stopping rule.

Step 1: vectorized simulation on the GPU. A single GPU call simulates a batch of annual maxima for many posterior draws and many AR6 paths at once:

1. **Prepare batch:**
   - on the CPU, sample a block of posterior draws and AR6 MSL paths,

- stack them into CuPy arrays

  `eta0_batch`, `eta1_batch`, `sigma_batch`, `xi_batch`, `X_batch_cm`

  with shape `(this_chunk, n_years)`.

2. **Simulate Poisson–GPD on GPU:** call

```
maxima_cm = simulate_annual_max_pp_batch_gpu(
    eta0_batch, eta1_batch, sigma_batch, xi_batch,
    X_batch_cm, u_cm
)
```

   where `maxima_cm` has shape `(this_chunk, n_years)`. Internally this function:

   - computes Poisson rates $\Lambda_{s,t} = \exp(\eta_0^{(s)} + \eta_1^{(s)} X_t^{(s)})$ via broadcasting,
   - draws Poisson counts $N_{s,t}$ and GPD excesses $Z_{s,t,i}$ on the GPU,
   - reduces to annual maxima $M_t^{(s)} = u + \max_i Z_{s,t,i}$ or u if no exceedance occurs.

All these operations are vectorized and executed on the device using CuPy, which provides a NumPy-like interface for CUDA arrays [Askar et al., 2024]. This turns the Monte Carlo step into a sequence of large dense array operations and random draws, which GPUs handle efficiently.

Step 2: damage evaluation and streaming accumulation. The batch of annual maxima is then converted to metres and mapped to damages for all candidate heights:

1. **Broadcast across heights:** convert to metres,

```
maxima_batch_m = maxima_cm / 100.0
```

   and form a 3d tensor of potential damage inputs,

```
exceedances = cp.where(
    maxima_batch_m[:, None, :] >= cand_heights_cp[None, :, None],
    maxima_batch_m[:, None, :],
    0.0,
)
```

   so that `exceedances` has shape `(this_chunk, C, n_years)`. Here:

   - if $M_t^{(s)} < h$, we set the entry to 0 (no flood damage),
   - if $M_t^{(s)} \geq h$, we pass the full water level $M_t^{(s)}$ into the damage curve.

2. **Map to monetary damages:** flatten `exceedances` to a 1d array on the GPU, apply a damage interpolator based on the Prahl curves to obtain damages in currency units, and reshape back to `(this_chunk, C, n_years)`.

3. **Reduce over scenarios and years:** sum over the first and last axes to get one damage total per candidate height for the current batch,

$$\Delta\_\text{damage}_h = \sum_{s,t} d_t(F_{s,t} \mid h).$$

4. **Update running totals:** on the CPU,

$$\texttt{cum\_damage}[h] \leftarrow \texttt{cum\_damage}[h] + \Delta\_\text{damage}_h$$

and

$$S \leftarrow S + \texttt{this\_chunk}.$$

The raw arrays `maxima_batch_m` and `exceedances` are then freed. At any time we only store $O(|\mathcal{H}_{\text{eff}}|)$ statistics: the cumulative damages and the scalar S.

Crucially, we never store the full matrix of historical samples $Y_{s,h}$. This is exactly why a CLT/normality-based workflow would be awkward here: to test for approximate normality at each height and to estimate higher moments reliably, we would either need to keep a large slice of the $Y_{s,h}$ history in memory or repeatedly resample from disk.

Step 3: confidence-based stopping (distribution-free). Every `check_every` batches we run a stopping check:

1. **Compute sample means:** for each $h \in \mathcal{H}_{\text{eff}}$,

$$\hat{\mu}_h(S) = C_n(h) + \frac{\texttt{cum\_damage}[h]}{S}.$$

2. **Compute confidence radius:** using Hoeffding's inequality and the bound $0 \le D(F \mid h) \le D_{\max}$, we evaluate

$$r(S) = D_{\max}\sqrt{\frac{1}{2S}\log\left(\frac{2|\mathcal{H}_{\text{eff}}|\,S(S+1)}{\delta}\right)},$$

which is the same radius as in (4).

3. **Identify empirical best:** set

$$\hat{h}(S) = \arg\min_{h \in \mathcal{H}_{\text{eff}}} \hat{\mu}_h(S).$$

4. **Stopping rule:** if

$$\hat{\mu}_{\hat{h}(S)}(S) + r(S) < \hat{\mu}_h(S) - r(S) \quad \text{for all } h \neq \hat{h}(S),$$

we stop and recommend $\hat{h}(S)$; otherwise we continue with the next batch.

This procedure is fully distribution-free: it does not assume that the $Y_{s,h}$ are approximately Gaussian, and it does not require us to estimate variances or higher moments. All we need is bounded one-year damage, which we already enforce via the damage curves. Because we only ever store running sums and counts, the algorithm can stream arbitrarily many Monte Carlo episodes through the GPU without running out of device memory, and the Hoeffding-based stopping rule provides a fixed-confidence guarantee on the recommended height. In short, instead of trying to force a CLT-based normal approximation to behave well for heavy-tailed damages (which would be statistically fragile and computationally expensive), we deliberately work with conservative, non-asymptotic bounds that align with our GPU-friendly, batch-streaming implementation.

4 Case Study: Halmstad

The methodology was applied to Halmstad, Sweden, using the damage and protection cost curves provided by Prahl et al. [2018].

4.1 Economic Inputs

The optimization relies on two key economic functions: the damage cost curve and the protection cost curve. Figure 10 illustrates the estimated economic damage as a function of flood depth. The curve is convex, indicating that damage costs accelerate with flood severity. Figure 11 shows the cost of constructing and maintaining levees of various heights.

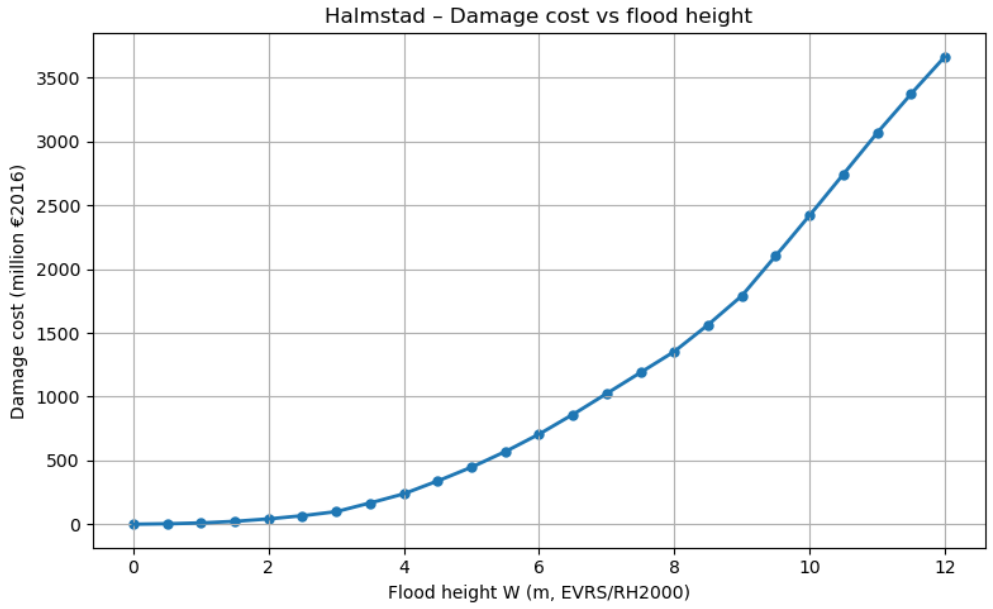

Figure 10: Damage cost curve for Halmstad. The y-axis represents the economic loss in Euros for a given flood level (x-axis).

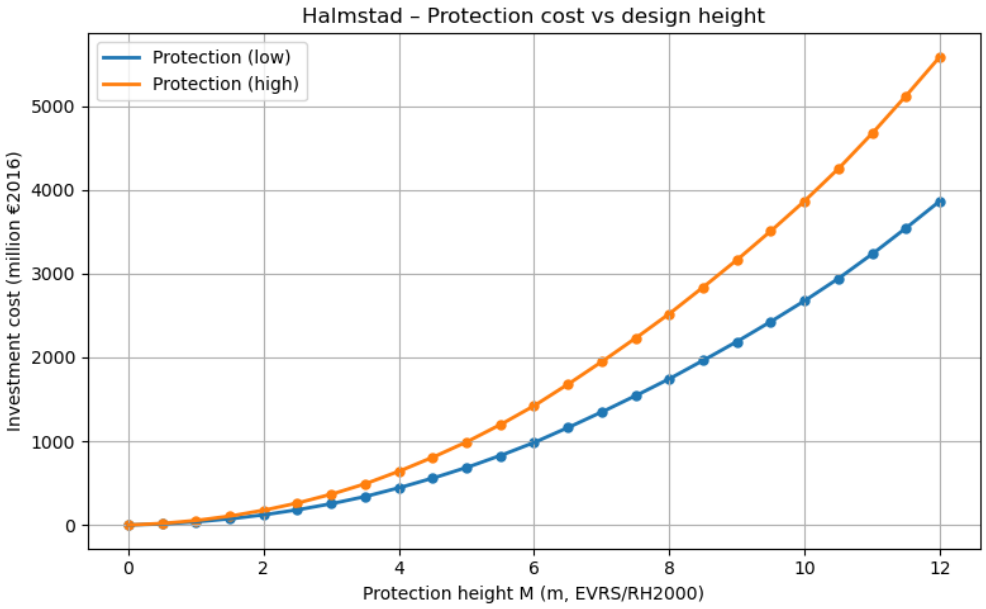

Figure 11: Protection cost curve for Halmstad. The y-axis represents the construction and maintenance cost in Euros for a levee of a given height (x-axis).

4.2 Results

The risk-neutral best-arm identification algorithm was applied to the Halmstad case study with a fixed confidence level of $\delta = 0.05$. In each Monte–Carlo episode the simulator generated one 76-year flood trajectory under one posterior draw of $(\eta_0, \eta_1, \sigma, \xi)$ and one AR6 sea-level path, and the resulting total discounted damages were recorded for every candidate height. Because the exploration phase is purely observational, the number of episodes S was allowed to increase until the confidence intervals for all heights were non-overlapping (cf. section 3). Below we summarise how the confidence radii evolved and how the final recommendation was obtained.

Convergence of confidence intervals. Figure 12 shows the decay of the half–width of the 99% confidence interval for the 3 m height over time on log–log axes. At early times the interval spans several orders of magnitude, but it shrinks roughly as a power law $\propto S^{-0.48}$ (see the dashed line in Figure 13), which is close to the $S^{-1/2}$ rate predicted by Hoeffding's inequality [Lattimore and Szepesvári, 2020]. The tail of the run (Figure 14) illustrates the practical challenge: even after about 6.2×10^9 Monte–Carlo episodes the confidence interval still has a width of about 36 cost units. This slow convergence arises from heavy tails in the damage distribution and the small differences in expected costs between heights.

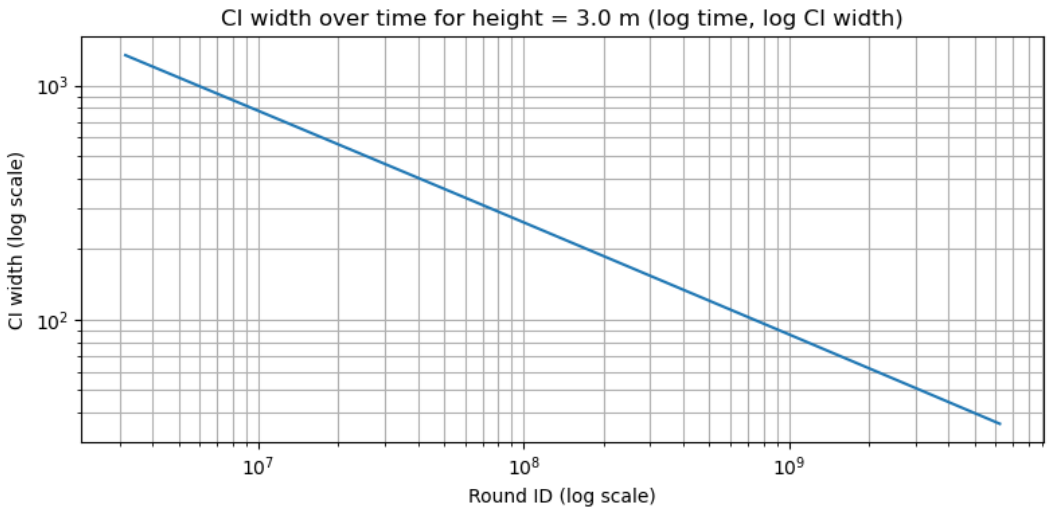

Figure 12: Evolution of the confidence interval half-width for the 3 m design on a log–log scale. The negative slope indicates a power-law decay in the number of Monte–Carlo episodes.

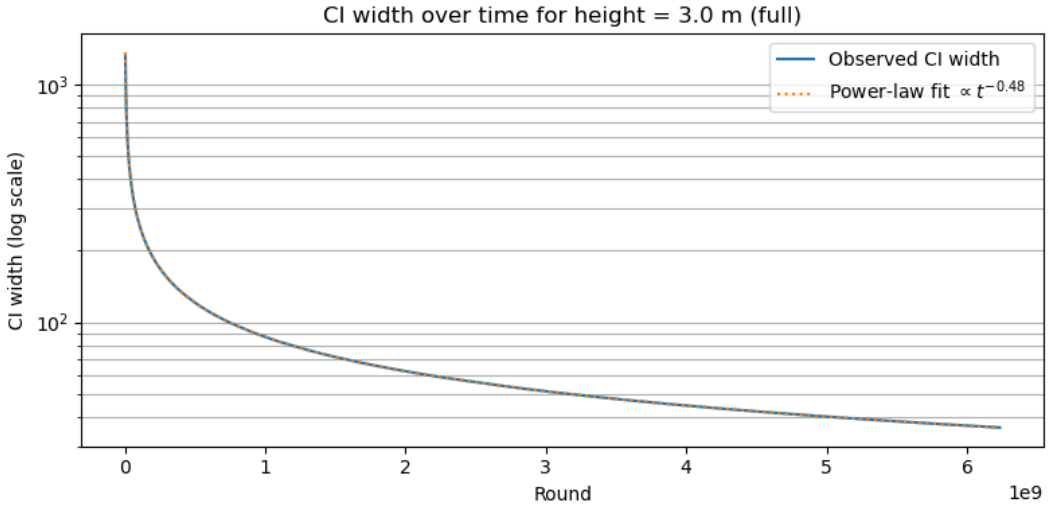

Figure 13: Observed confidence interval width for the 3 m height (solid blue) together with a fitted power-law decay $\propto S^{-0.48}$ (dashed orange). The nearly parallel lines on the log scale indicate that the empirical rate agrees well with the theoretical $S^{-1/2}$ convergence predicted by Hoeffding bounds.

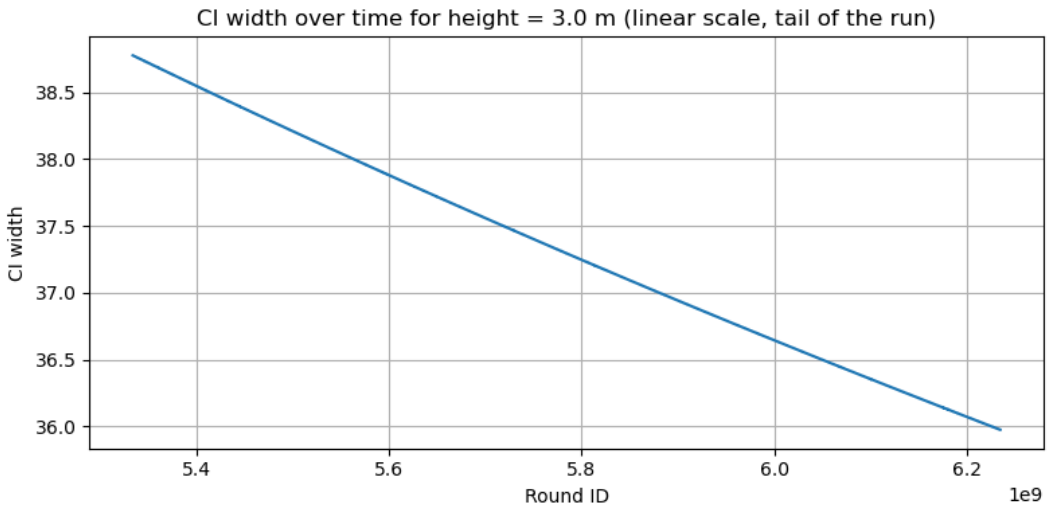

Figure 14: Tail behaviour of the confidence interval half-width for the 3 m design. Even at very large sample sizes the interval remains on the order of tens of cost units, illustrating the difficulty of resolving near-optimal heights under heavy-tailed damages.

Ranking of candidate heights. After approximately 6.234×10^9 episodes the stopping criterion was satisfied and the algorithm recommended the 3 m height. Figure 15 displays the five heights with the lowest estimated total costs at the final round along with their uncertainty intervals. The 3 m design has an expected total cost of about 6.7×10^2 monetary units (after discounting), while the second–best height, 2.5 m, is higher by only around 4×10^1 units. The next candidates (3.5 m and 4 m) are progressively more expensive due to both higher construction costs and diminishing flood damage reduction. The 2 m height is the worst because it fails to prevent many damaging floods. Although the differences between the two best designs are small relative to the heavy-tailed variability, the confidence intervals do not overlap at the stopping time, guaranteeing that the recommendation is correct with probability at least $1 - \delta$.

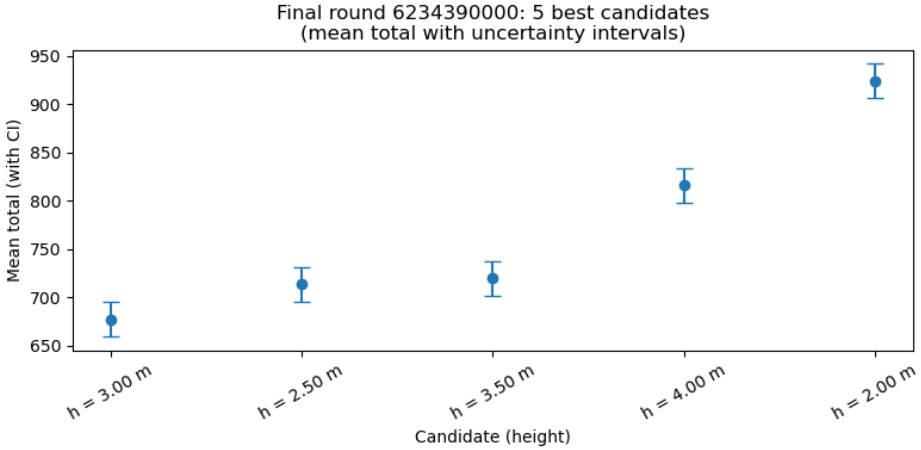

Figure 15: Mean total cost (points) and confidence intervals (vertical bars) for the five most competitive heights at the stopping time. The 3 m design has the lowest expected cost, with 2.5 m a close runner–up. Higher and lower designs are less economical.

Separation between the top two designs. To understand why the algorithm required billions of episodes, we track the separation between the upper confidence bound for the 3 m height and the lower bound for the 2.5 m height, shown in Figure 16. The gap decays monotonically and crosses zero only near 6.23×10^9 episodes. The zoomed-in view in Figure 17 reveals that just before crossing zero the difference is less than 0.2 cost units. Consequently the stopping time is driven by the need to detect minute differences in expected cost under heavy-tailed uncertainty. Once the separation becomes negative, the algorithm stops and selects the 3 m height.

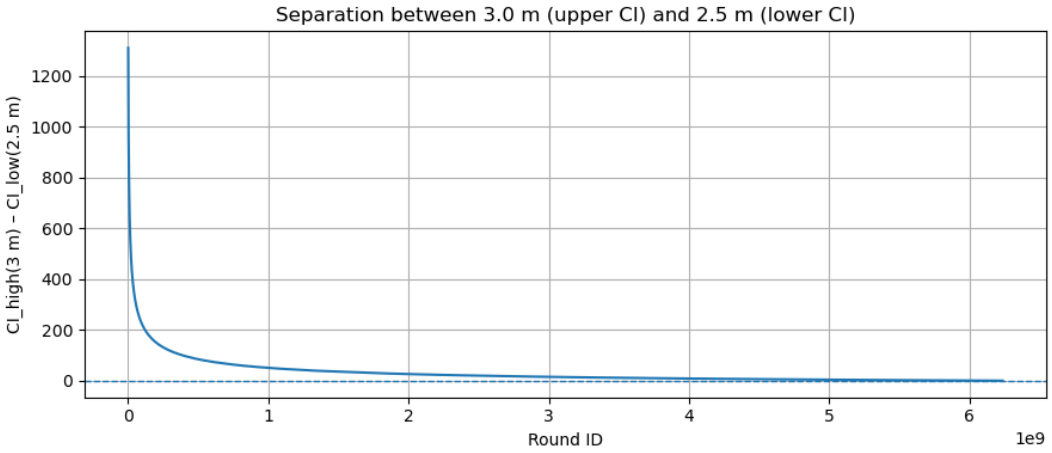

Figure 16: Evolution of the difference between the upper confidence bound for the 3 m height and the lower bound for the 2.5 m height. The dashed horizontal line marks zero. The gap shrinks over time and crosses zero only after $\approx 6.23 \times 10^9$ episodes.

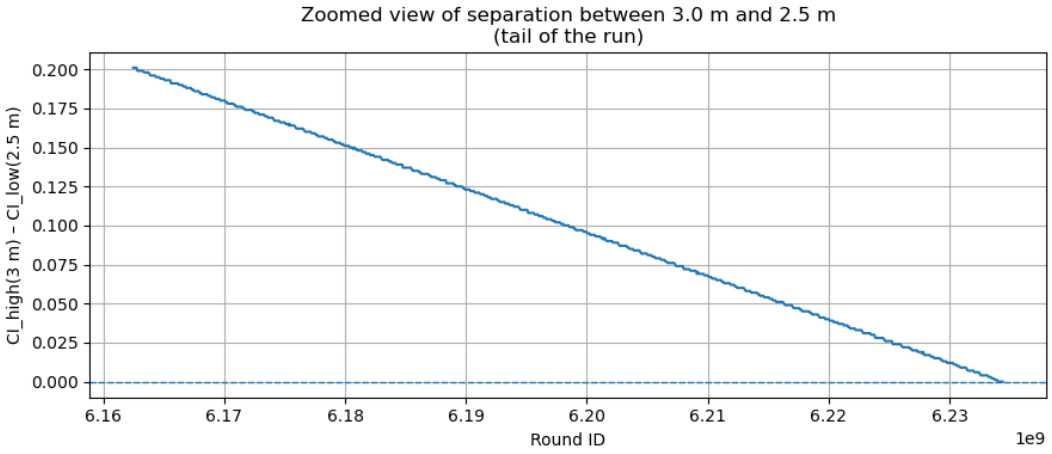

Figure 17: Zoomed view of Figure 16 near the end of the run. The separation between the confidence bounds is less than 0.2 cost units just before crossing zero, underscoring the algorithm's ability to resolve extremely small differences in expected cost.

Discussion. Overall, the confidence–based pure-exploration algorithm successfully identifies the risk–neutral optimal levee height while providing rigorous finite-sample guarantees on its recommendation. The heavy-tailed nature of extreme sea-level damages, coupled with the small gap

between the top designs, results in extremely slow convergence; more than six billion Monte–Carlo episodes were needed to confidently separate the best arm. These results highlight both the statistical efficiency of the algorithm and the computational cost of achieving high confidence in coastal adaptation under deep uncertainty.

5 Alternative Approach: Pairwise Optimization via Dueling Bandits

The fixed-confidence pure exploration approach described in Section 3 relies on the boundedness of the damage function ($D_{\max}$) to construct Hoeffding intervals. While rigorous, the convergence of this method is slow due to the high variance induced by the heavy-tailed flood distribution.

To address the computational bottleneck, we investigated an alternative formulation based on the *Dueling Bandits* framework [**?**]. Instead of estimating the absolute expected cost μ_h, this approach seeks to identify the "Condorcet winner"—the design height that is cheaper than any other design with probability greater than 0.5 in a random scenario.

5.1 Bayesian Beta-Dueling Algorithm

We employ a Bayesian Beta-Dueling algorithm, specifically adapted for the fixed-confidence setting. Let $\mathcal{H} = \{h_1, \dots, h_K\}$ be the set of candidate levee heights. For every pair of distinct candidates (h_i, h_j), we define the pairwise win probability p_{ij} as the probability that height h_i incurs a lower total cost than height h_j in a randomly sampled scenario (climate path and storm surge realization):

$$p_{ij} := \mathbb{P}(\text{Cost}(h_i) < \text{Cost}(h_j)). \tag{6}$$

Note that $p_{ji} = 1 - p_{ij}$ (ignoring ties, which are handled by splitting the mass). We model our uncertainty about these probabilities using Beta distributions. For each pair (i, j) with $i < j$, we maintain a posterior:

$$p_{ij} \sim \text{Beta}(\alpha_{ij}, \beta_{ij}), \tag{7}$$

where α_{ij} counts the number of scenarios where h_i was cheaper than h_j, and β_{ij} counts the reverse.

Algorithm Procedure. The algorithm proceeds in rounds $s = 1, 2, \dots$. In each round:

1. **Simulation:** We generate a single flood scenario F_s (including climate path and annual maxima) and compute the total cost $L_{s,k}$ for every candidate $h_k \in \mathcal{H}$.

2. **Update:** For every pair (i, j), we update the hyperparameters:

$$\alpha_{ij}^{(s)} = \alpha_{ij}^{(s-1)} + \mathbb{I}(L_{s,i} < L_{s,j}) + 0.5 \cdot \mathbb{I}(L_{s,i} = L_{s,j}), \tag{8}$$

$$\beta_{ij}^{(s)} = \beta_{ij}^{(s-1)} + \mathbb{I}(L_{s,i} > L_{s,j}) + 0.5 \cdot \mathbb{I}(L_{s,i} = L_{s,j}). \tag{9}$$

3. **Stopping Rule:** We employ a probabilistic relaxation of the Copeland winner criterion. We compute the posterior probability that h_i is better than h_j (i.e., $p_{ij} > 0.5$):

$$P_{ij}^{(s)} := \mathbb{P}(p_{ij} > 0.5 \mid \mathcal{D}_s) = I_{0.5}(\beta_{ij}^{(s)}, \alpha_{ij}^{(s)}), \tag{10}$$

where $I_x(a, b)$ is the regularized incomplete beta function (the CDF of the Beta distribution). Note that $I_{0.5}(\beta, \alpha)$ corresponds to the survival function at 0.5.

We then define the "confidence score" for each candidate i as its worst-case pairwise superiority:

$$q_i^{(s)} := \min_{j \neq i} P_{ij}^{(s)}. \tag{11}$$

The candidate with the highest score is the current empirical winner: $i_s^* = \arg\max_i q_i^{(s)}$.

The algorithm terminates when we are confident that i^* beats *all* other candidates with probability > 0.5. Specifically, we stop when:

$$q_{i_s^*}^{(s)} \geq 1 - \delta, \tag{12}$$

where δ is the user-defined error tolerance (e.g., 0.05).

5.2 Empirical Performance and Convergence

Applied to the Halmstad dataset, the Beta-Dueling algorithm demonstrates extreme computational efficiency. The method converges to a selected height of $h = 2.50\,\text{m}$ in fewer than 2,000 simulation rounds with a confidence of $\delta = 0.05$. In contrast, the mean-based estimation required significantly larger sample sizes to separate the top candidates.

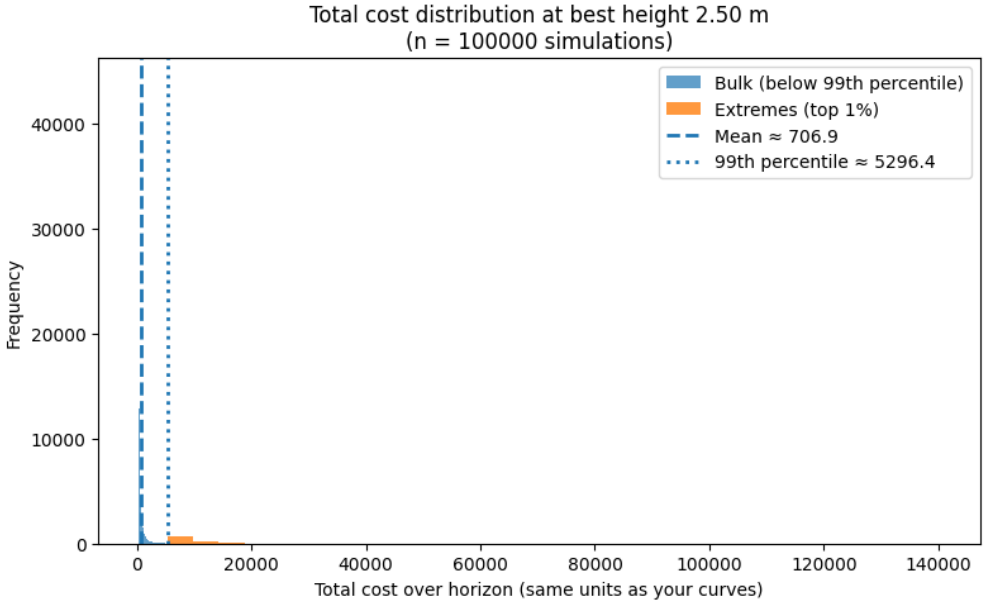

Figure 18: Convergence of the Dueling Bandit algorithm. The plot shows the evolution of the confidence score q_i for the leading candidates. The algorithm stops when the top candidate's minimum pairwise win probability exceeds $1 - \delta$ (0.95).

5.3 Theoretical Limitations

Despite its speed, our analysis reveals that the Dueling Bandit framework is fundamentally misaligned with the risk-neutral objective defined in Eq. (1) for heavy-tailed hazard domains.

The Dueling Bandit optimizes for the *probability* of winning, effectively selecting the median-optimal solution rather than the mean-optimal solution. In the context of flood protection, this leads to a phenomenon we term "Magnitude Blindness." Consider a comparison between a lower, "risky" levee (h_{low}) and a higher, "safe" levee (h_{high}):

1. **High Probability Scenarios:** In the vast majority of years (e.g., 99%), extreme surges do not occur. The lower levee incurs lower construction costs ($C(h_{low}) < C(h_{high})$) and zero damage. Thus, h_{low} "wins" the pairwise duel.

2. **Low Probability Scenarios:** In rare tail events (e.g., 1%), a catastrophic surge overtops h_{low} but not h_{high}. The damage difference is immense ($D \approx D_{\max}$), making h_{high} significantly cheaper in these specific instances.

Because the Beta-Dueling update step treats a "win" by €1 the same as a "win" by €1,000,000, it effectively ignores the magnitude of the loss in the tail.

Consequently, the Dueling Bandit selected $h = 2.50\,\text{m}$, which has a mean total cost of approximately 706 M€. However, the comprehensive mean-estimation described in Section 4 identified $h = 3.00\,\text{m}$ as the global optimizer with a mean cost of 677 M€. The Dueling Bandit failed to account for the catastrophic tail risks that justify the additional capital expenditure of the 3.00 m wall. Therefore, while ordinal optimization methods are computationally attractive, they are unsuitable for risk-neutral planning under heavy-tailed distributions.

6 Conclusion

This study has presented a computational framework for optimizing coastal adaptation strategies under deep uncertainty, utilizing the Multi-Armed Bandit (MAB) paradigm to navigate the complex interplay between epistemic climate uncertainty and aleatoric flood extremes. By applying this framework to the case study of Halmstad, Sweden, using IPCC AR6 sea-level projections, we have highlighted the critical importance of algorithmic selection in the design of resilient infrastructure.

Our primary finding is the identification of a fundamental trade-off between computational efficiency and risk-neutral accuracy in heavy-tailed domains. The Bayesian Beta-Dueling algorithm, while converging orders of magnitude faster than mean-based estimation, exhibited *Magnitude Blindness*. By optimizing for the probability of lower cost rather than the expected magnitude of cost, the Dueling Bandit approach effectively selected a median-optimal design ($h = 2.50$ m) rather than the mean-optimal design ($h = 3.00$ m). This resulted in a recommendation that, while cheaper in typical years, failed to account for the catastrophic damages associated with low-probability, high-impact tail events.

Conversely, the Confidence-Based Pure Exploration algorithm, grounded in Hoeffding's concentration inequalities for bounded damages, successfully identified the risk-neutral optimal height of 3.00 m. Although this method required over 6×10^9 Monte Carlo episodes to resolve the small differences in expected cost amidst high variance, it provided a rigorous, finite-sample guarantee of optimality. The 3.00 m design justifies its higher capital cost by effectively truncating the ruinous tail of the damage distribution—a benefit that ordinal optimization methods systematically ignore.

These results offer a cautionary tale for the application of machine learning in climate risk management. Algorithms that rely on pairwise comparisons or win-probabilities are prone to maladaptation when loss distributions are fat-tailed. For coastal defense planning in the Anthropocene, where the "risk" is dominated by the extremities of the distribution, optimization methods must explicitly integrate the magnitude of potential damages. We conclude that while pure exploration is computationally demanding, it is a reliable path to identifying truly robust adaptation strategies that protect against the deep uncertainty of future sea levels.

References

L. M. Abadie, I. Galarraga, A. Markandya, and E. Sainz de Murieta. Risk measures and the distribution of damage curves for 600 european coastal cities. *Environmental Research Letters*, 14(06):064021, 2019. doi: 10.1088/1748-9326/ab185c.

Oriol Abril-Pla, Virgile Andreani, Colin Carroll, Larry Dong, Christopher J. Fonnesbeck, Maxim Kochurov, Ravin Kumar, Junpeng Lao, Christian C. Luhmann, Osvaldo A. Martin, Michael Osthege, Ricardo Vieira, Thomas Wiecki, and Robert Zinkov. PyMC: A modern and comprehensive probabilistic programming framework in Python. *PeerJ Computer Science*, 9(e1516), 2023. doi: 10.7717/peerj-cs.1516.

Tair Askar, Argyn Yergaliyev, Bekdaulet Shukirgaliyev, and Ernazar Abdikamalov. Exploring numba and cupy for gpu-accelerated monte carlo radiation transport. *Computation*, 12(3):61, 2024. doi: 10.3390/computation12030061.

Gregory G. Garner, Tim H. J. Hermans, Robert E. Kopp, Aimee B. A. Slangen, Tasmin L. Edwards, Anders Levermann, Sophie Nowicki, Matthew D. Palmer, Chris Smith, Baylor Fox-Kemper, Helene T. Hewitt, Cunde Xiao, and et al. IPCC AR6 Sea Level Projections (version 20210809) [data set], 2021. URL `https://doi.org/10.5281/zenodo.5914709`. Sea-level projections associated with the IPCC Sixth Assessment Report, including global Monte Carlo samples and regional relative sea-level projections.

joensson12. flood_bandit. `https://github.com/joensson12/flood_bandit`, 2025.

Tor Lattimore and Csaba Szepesvári. *Bandit Algorithms*. Cambridge University Press, 2020. Chapter 33 provides an accessible introduction to pure exploration and fixed-confidence best-arm identification.

Boris F. Prahl, Markus Boettle, Luís Costa, Jürgen P. Kropp, and Diego Rybski. Damage and protection cost curves for coastal floods within the 600 largest european cities. *Scientific Data*, 5:180034, 2018. doi: 10.1038/sdata.2018.34.